Capacitance and Field-Driven Electron Transport in Electrochemically Self-Assembled Nanoporous ZnO/Dye Hybrid Films

Torsten Oekermann,*,† Tsukasa Yoshida,‡ Cathrin Boeckler,† Jürgen Caro,† and Hideki Minoura‡

Institute of Physical Chemistry and Electrochemistry, University of Hannover, Callinstrasse 3-3A, 30167 Hannover, Germany, and Graduate School of Engineering, Gifu University, Yanagido 1-1, Gifu 501-1193, Japan

Received: March 17, 2005; In Final Form: May 3, 2005

Electrodeposited nanoporous ZnO/eosin Y hybrid films have been investigated in view of their potential applications in dye-sensitized solar cells and supercapacitors. Intensity-modulated photocurrent spectra were measured at different electrode potentials at films of different thicknesses. It was found that the results represent either the *RC* constant of the cell and surface recombination of photogenerated holes with electrons or the diffusion of photogenerated electrons and are dependent on the electron concentration in the ZnO, which is influenced by the film thickness, the electrode potential, and the light intensity. The results suggest that the porosity of the electrodeposited ZnO increases with the film thickness and the films therefore consist of two parts, a less porous part deposited in the first few minutes that exhibits field-driven electron transport and a more porous outer part where electron transport is by diffusion. The results are supported by frequency-dependent capacitance measurements, which also show that the material is suitable for supercapacitors.

1. Introduction

Cathodic electrodeposition of ZnO from aqueous zinc salt solutions in the presence of oxidants such as O_2, H_2O_2, or NO_3^- and water-soluble dye molecules is a valuable new route for the one-step preparation of new inorganic/organic hybrid materials for dye-sensitized solar cells.[1] Dye molecules with acid groups such as $-COO^-$ and $-SO_3^-$ were found to adsorb to the growing oxide film and influence its structure and morphology. At the same time, they can function as sensitizers in the deposited films. Highly porous ZnO was obtained especially in the presence of O_2 and the red xanthene dye eosin Y, which was investigated in view of an application in dye-sensitized solar cells.[2−4] A study with intensity-modulated photocurrent spectroscopy (IMPS) and intensity-modulated voltage spectroscopy (IMVS) proved the very high electron collection efficiency of these films, which is caused by a remarkably fast electron transport due to the absence of grain boundaries and the high crystallinity of the electrodeposited material.[5] However, dye aggregation in the pores of the as-deposited films led to quenching of photogenerated electrons and therefore to a low electron injection efficiency. For this reason, the overall efficiency of the as-electrodeposited films was still low compared to colloid-processed nanoparticulate ZnO films. The problem could be solved by the desorption and readsorption of the dye, leading to the formation of a dye monolayer on the inner surface of the porous ZnO film and thus to a significant improvement of the electron injection efficiency.[6] As expected from their higher electron collection efficiency, the performance of electrodeposited ZnO films surpassed that of colloid-processed ZnO films after the readsorption process.

Although IMPS and IMVS provided a valuable explanation for the high performance of electrodeposited ZnO/dye films after readsorption of the dye, more detailed investigations are still necessary to fully understand the electrochemical and photoelectrochemical properties of these new materials as well as their relation with structural properties and ways to influence them, also in view of other applications such as electronics and photoelectronics. For example, although an IMPS response typical for electron transport by diffusion was found for as-deposited ZnO/eosin Y films,[5] the question remained if there is still a certain contribution by field-driven electron transport since ZnO prepared by cathodic electrodeposition is known to have a rather high doping level.[7] This might enable a higher penetration depth of the electric field into the nanoporous layer compared to nanoparticulate TiO_2 films, where the field is believed to penetrate into the first monolayer of TiO_2 nanoparticles (typically 25 nm) or less.[8] To address this question, potential-dependent IMPS measurements at electrodeposited ZnO/eosin Y films of different film thicknesses have been performed in this study. Since as-deposited ZnO/eosin Y films were found to lose a part of their dye content during photoelectrochemical measurements,[5] films with readsorbed dye have been used due to their higher and more stable performance.

In addition, capacitance measurements have been made to supplement and interpret the results of the IMPS measurements. Besides readsorbed films, pure ZnO films with desorbed dye have also been used for this purpose. Capacitance measurements would also be useful in view of applications as supercapacitors,[9] for which electrodeposited ZnO/dye films might be suitable due to their rather low pore sizes of down to about 10 nm.[5]

* Author to whom correspondence should be addressed. Phone: +49-511-7624270. Fax: +49-511-76219121. E-mail: torsten.oekermann@pci.uni-hannover.de.

† University of Hannover.

‡ Gifu University.

10.1021/jp051394p CCC: $30.25
Published on Web 06/02/2005

2. Theory

In the limit of small-amplitude light perturbations, the generation and collection of electrons in dye-sensitized nanoporous films can be described by the continuity equation[10]

$$\frac{\partial n}{\partial t} = \Phi_{inj}\alpha I_0 \, e^{-\alpha x} + D_n\frac{\partial^2 n}{\partial x^2} - \frac{n - n_0}{\tau_n} \quad (1)$$

where Φ_{inj} is the injection efficiency for electrons from the lowest unoccupied molecular orbital (LUMO) of the dye molecule into the conduction band of the n-type semiconductor, α is the absorption coefficient, I_0 is the incident light intensity, D_n is the effective (intensity-dependent) diffusion coefficient of electrons, n is the electron density under illumination, n_0 is the equilibrium electron concentration in the dark, and τ_n is the effective first-order electron lifetime. The electron lifetime is assumed to be determined by the back-reaction of electrons with the oxidized species in the electrolyte, which is I_3^- in case of the most commonly used iodide/iodine redox couple[11] which is also used in this study. Light scattering and any electric field in the film are usually neglected.[12,13]

During IMPS measurements, the cell is illuminated with sinusoidally modulated light with a small alternating current (ac) component (10% or less of the direct current (dc) component) of various frequencies f. The photocurrent response is measured in terms of its amplitude and phase shift with respect to the modulation of the incident light. They are usually presented in complex plane plots or in the so-called Bode plots, which show the amplitudes and phase shifts versus the measuring frequencies. Analytical solutions of eq 1 for a sinusoidal modulation of the light with $I(t) = I_0[1 + (\delta\, e^{i\omega t})]$ under short-circuit conditions are known from the literature.[12,13] The normalized solution for illumination from the electrolyte side is

$$\frac{j_{photo}}{q\delta\Phi_{inj}I_0} = \frac{\alpha}{\alpha+\gamma}\,\frac{e^{(\gamma-\alpha)d} - e^{-(\gamma+\alpha)d} + 2\alpha\dfrac{e^{(\gamma-\alpha)d}-1}{\gamma-\alpha}}{e^{\gamma d} + e^{-\gamma d}} \quad (2)$$

with

$$\gamma = \left[\frac{1}{D_n\tau_n} + i\frac{\omega}{D_n}\right]^{1/2} \quad (3)$$

where q is the elementary charge, d is the film thickness, and $\omega = 2\pi f$ is the modulation frequency.[14] It describes a (flattened) semicircle in the positive/negative quadrant of the complex plane. From f_{min}, the frequency of the minimum of the semicircle, the electron transit time $\tau_D = 1/\omega_{min} = {}^1/_2\pi f_{min}$ can be calculated, which gives a convenient estimate of the average time that photoinjected electrons need to reach the back-contact.

The experimentally measured IMPS response is affected by *RC* attenuation, especially toward higher frequencies. To obtain the attenuated response, eq 2 is multiplied with the complex attenuation function

$$A(\omega) = \frac{1}{1 + i\omega RC} \quad (4)$$

where R is the series resistance and C is the capacitance of the electrode.[15] For nanoparticulate TiO_2 films, it has been found that under short-circuit conditions R and C are due to the conductive substrate and its interfaces with the electrolyte and the semiconductor film with typical values of around 20 Ω and 30 μF cm^{-2}, respectively.[14,15]

The IMPS response of bulk semiconductor electrodes, where a space charge layer exists and electron transport is driven by an electric field, is quite different from that of nanoporous electrodes. Since electron transport is much faster, the IMPS response in the positive/negative quadrant only reflects the *RC* attenuation not electron transport. Furthermore, surface recombination of photogenerated minority carriers with majority carriers is often seen at bulk electrodes. The surface recombination can also be detected as a semicircle in the positive/positive quadrant of an IMPS complex plane plot toward low frequencies. In a simple model, which considers either recombination or charge transfer as the only two alternatives of minority carriers at the electrode surface, the IMPS response can be described by[12]

$$\frac{j_{photo}}{qg_{ac}} = \frac{k_{tr} + i\omega}{k_{rec} + k_{tr} + i\omega} \quad (5)$$

where k_{tr} and k_{rec} are the rate constants of charge transfer and recombination and g_{ac} is the ac component of the Gärtner flux, which is the flux of photogenerated minority carriers through the space charge layer to the electrode surface. While the imaginary component of this function tends to 0 in the high-frequency limit ($\omega \rightarrow \infty$) as well as in the low-frequency limit ($\omega \rightarrow 0$), the real component tends to 1 ($\omega \rightarrow \infty$) and $k_{tr}/(k_{tr} + k_{rec})$ ($\omega \rightarrow 0$).[12] Both k_{tr} and k_{rec} are pseudo-first-order rate constants that depend on the concentration of electroactive species in the electrolyte (k_{tr}) or the concentration of majority carriers at the electrode surface (k_{rec}). It is also important to note that

$$k_{tr} + k_{rec} = \omega_{max} = 2\pi f_{max} \quad (6)$$

where f_{max} denotes the frequency of the maximum of the semicircle.

3. Experimental Section

3.1. Film Preparation and Characterization. Details of the electrochemical self-assembly of ZnO/eosinY films from $ZnCl_2$/O_2 aqueous solutions are given in ref 4. For this study, ZnO films were electrodeposited from a solution containing 5 mM $ZnCl_2$ (Merck), 0.1 M KCl (Merck), and 50 μM eosinY disodium salt (Kanto Chemicals) that was saturated with oxygen and maintained at 70 °C. F-doped SnO_2 (FTO)-coated conducting glass (Nippon Soda Glass, 20 Ω/square) served as the substrate. To obtain reproducibly homogeneous films with the same thicknesses for a certain deposition time, a rotating disk electrode (Radiometer BM-EDI101) operating at 500 rpm was used as the working electrode. The electrodeposition was carried out at −1.0 V vs a standard calomel electrode (SCE) using a potentiostat (Hokuto Denko HSV-100) and a 4 N pure Zn wire as the counter electrode. Deposition times were varied between 2 and 20 min. The deposited films were rinsed with water and dried under air at room temperature. For desorption of the dye, the as-deposited films were soaked in a dilute aqueous KOH solution (pH = 10.5) for about 12 h. Readsorption of eosin Y was carried out by refluxing in a 0.5 M ethanolic dye solution for 1 h. Film thickness measurements were made with a Sloan Dektak 3030 ST profilometer.

3.2. Photoelectrochemical and Impedance Measurements. Electrodes with geometrical film areas of 0.12 cm^2 were prepared from the as-deposited, desorbed, and readsorbed films. All measurements were made in a three-electrode setup with the ZnO or ZnO/eosinY electrode as the working electrode, a

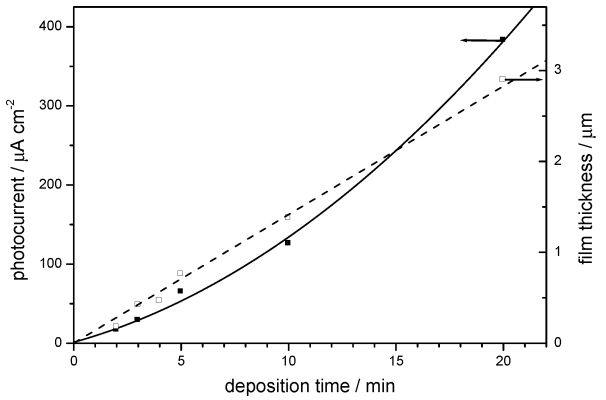

Figure 1. Film thickness (- -□- -) and dc photocurrents (−■−) of ZnO/eosin Y films prepared in different deposition times. The photocurrents were measured after readsorption of eosin Y at 0 V vs Ag/Ag^+ with green LED light of 0.8 mW cm^{-2}.

Pt wire as the counter electrode, and an Ag/Ag^+ reference electrode. The Ag/Ag^+ electrode consisted of an Ag wire in a 0.01 M solution of $AgNO_3$ in acetonitrile, which had a potential of +0.27 V vs SCE as confirmed by measuring the redox potential of the ferrocene/ferricenium redox couple.

High-intensity green light-emitting diodes (LEDs; 530 nm), which provided dc light intensities of up to 2.6 mW cm^{-2} (8.6×10^{15} photons s^{-1} cm^{-2}) at the electrodes, were used as light sources for IMPS. The ZnO films were illuminated from the electrolyte side through a quartz window, modulating the light intensities (±5%) by an ac voltage applied to the LED via a series resistor from an NF Electronic Instruments S-5720C frequency response analyzer (FRA). The light intensities were measured with a calibrated Eppley thermopile. Neutral density filters were used to vary the light intensities down to about 0.2 mW cm^{-2}. A Toho Technical Research 2000 potentiostat/galvanostat was used to measure the photocurrents. The electrolyte was 0.5 M tetrapropylammonium iodide in a mixture of acetonitrile and ethylene carbonate (1:4 w/w). Iodine was not used to avoid light absorption in the electrolyte. Due to the low light intensity used in this study, only small amounts of I_3^- are expected to develop during the experiments. Furthermore, electrolyte of a rather high volume of 20 mL was used, which showed hardly any coloration even after several hours of experiments.

Experimental IMPS results were fitted using the least-squares fitting routine of Origin 6.1, after splitting the complex functions used for fitting into their real and imaginary components.

Impedance measurements were made with a Zahner IM6e electrochemical workstation, using the same three-electrode setup. Tetrabutylammonium perchlorate (TBAP) was used as supporting salt, while the solvent (acetonitrile + ethylene carbonate) was the same as that used in the photoelectrochemical experiments.

4. Results and Discussion

4.1 Film Thickness and Morphology. Figure 1 shows the relation between deposition time, film thickness, and the dc photocurrents measured during the IMPS measurements. While the dependence of the film thickness on the deposition time appears to be almost proportional, a slightly overproportional increase is found for the photocurrent. This is quite astonishing because according to the Lambert−Beer law the intensity of the light on its way through the film should decrease exponentially, provided that the dye distribution is homogeneous throughout the film. It should be remembered, however, that the films are illuminated from the electrolyte side in this study. The experimental result can be understood if an increasing dye concentration in the film with increasing deposition time is assumed. This increase in the dye concentration obviously not only compensates but overcompensates for the effect of the Lambert−Beer law.

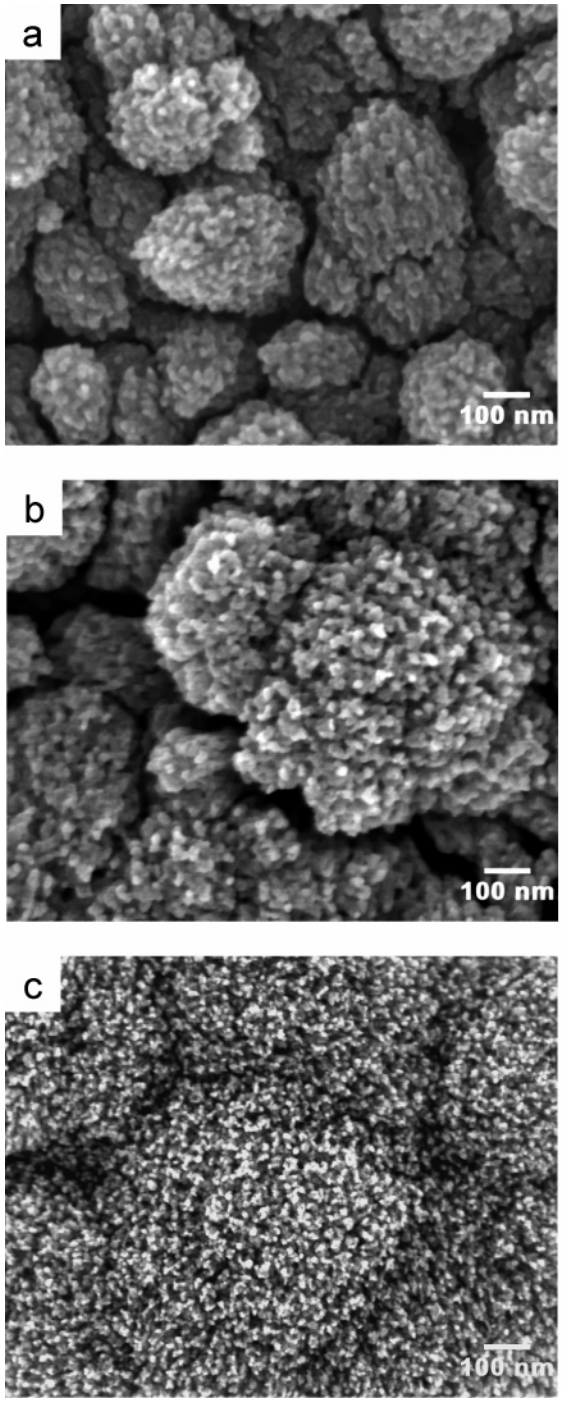

Figure 2. SEM of ZnO/eosin Y films electrodeposited for (a) 2, (b) 5, and (c) 20 min after desorption of the dye with dilute aqueous KOH.

The reason for the increasing dye concentration with increasing film thickness can be seen in Figure 2. The scanning electron microscopy (SEM) images show films electrodeposited for 2, 5, and 20 min after desorption of the dye. As reported earlier,[4] the films consist of domains that can be described as porous single crystals and that can be clearly seen in Figure 2. It can also be seen that these domains become larger with increasing deposition time. At the same time, the domains and therefore

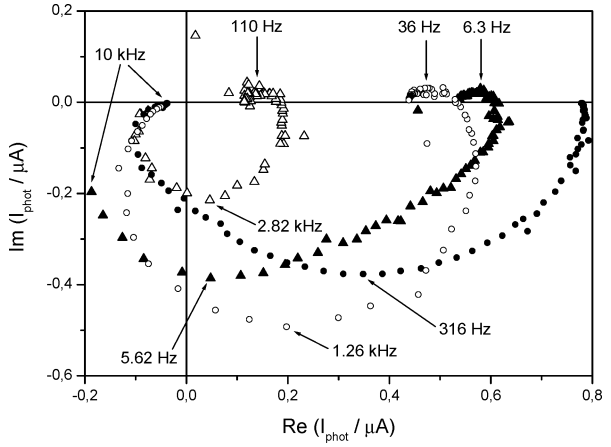

Figure 3. IMPS complex plane plots of ZnO/eosinY films with readsorbed dye deposited in 2 and 10 min at two different electrode potentials. For better visibility, three of the plots are shown enlarged to different scales: (●) deposited in 10 min, measured at 0 V vs Ag/Ag+, shown to scale; (○) 10 min, −0.8 V, 10 times enlarged; (▲) 2 min, 0 V, 3 times enlarged; (△) 2 min, −0.8 V, 30 times enlarged.

the whole film become considerably more porous. The increased porosity will lead to a higher dye concentration if monolayer coverage of the ZnO surface is assumed throughout the film.

4.2. IMPS Measurements. IMPS was conducted between −0.8 and 0 V vs Ag/Ag^+ with films prepared for deposition times between 2 and 20 min. Some examples for IMPS complex plane plots are shown in Figure 3. Both plots for the film deposited in 2 min show semicircles not only in the positive/negative quadrant according to eq 2 or 4 but also in the positive/positive quadrant toward low frequencies. The latter indicates a behavior like that of a bulk electrode with a recombination reaction of photogenerated holes at the electrode surface (eq 5). Since green light was used in the IMPS experiments, which means that no holes are photogenerated in the ZnO since it does not absorb visible light, the photogenerated holes are probably located in the dye molecules. Very high f_{min} values far above 1 kHz are also typical for a bulk electrode, with f_{min} reflecting the *RC* constant of the cell (eq 4).

With increased deposition time for the film, the IMPS results become increasingly potential-dependent. If measured at −0.8 V vs Ag/Ag^+, then the IMPS behavior of the film deposited in 10 min is similar to that of the film prepared in 2 min, i.e., the behavior of a bulk electrode with a semicircle in the positive/positive quadrant. Considering that f_{min} in this plot reflects the *RC* constant, the IMPS response was fitted with eq 4 with both *C* and *R* as adjustable parameters. At first glance, the fits, which are seen as dashed lines in Figure 4a, are not quite satisfying. Deviations at lower frequencies are obviously due to the surface recombination, which is seen in a much better fit below 1 kHz if a product of eqs 4 and 5 is used as the fit function (solid lines in Figure 4a). In the latter case, *C* and *R* (eq 4) as well as k_{tr} and k_{rec} (eq 5) were adjustable parameters. Deviations at higher frequencies are probably caused by a delay in the light response of the LED with respect to the applied voltage. Such a delay leads to a higher experimental phase shift, which is reflected by negative real components in Figure 4a and in a diversion of the plot through the negative/negative quadrant in Figure 3. However, despite such deviations, even the fits with the simplest model (eq 4) yield very reasonable *R* values of 21.5 Ω for the real component and 20.7 Ω for the imaginary component. These values are in very good agreement with each other and also with simple resistivity measurements of the conductive glass substrate with a multimeter. These measurements gave values of around 20 Ω for a distance of 1 cm between the measuring electrodes, which reflects the distance between the contact with the copper cable and the ZnO films in the electrodes used for the IMPS measurements. *C* values of 6.5 and 6.3 μF were obtained from the fits.

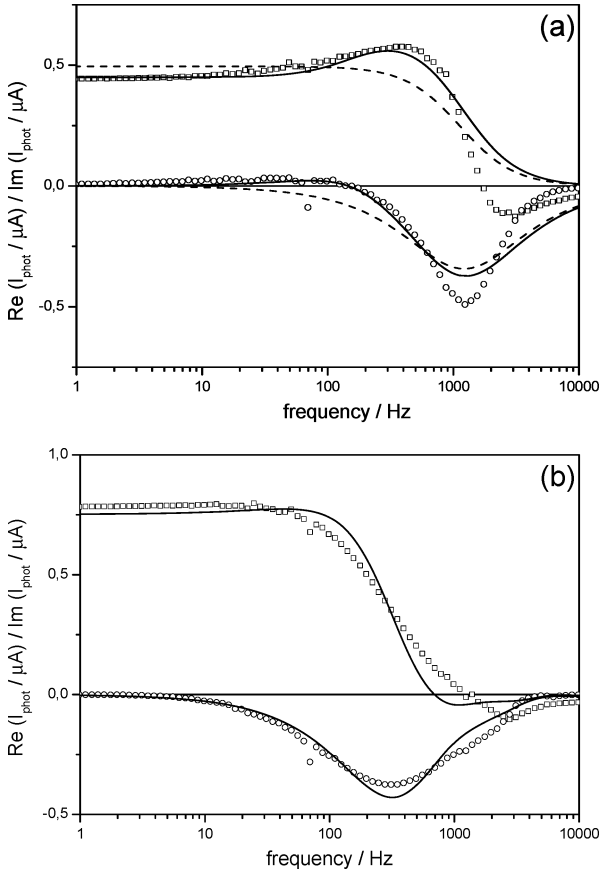

Figure 4. Bode plots of experimental IMPS results (□, real components; ○, imaginary components) and their fits (lines) for a ZnO/eosin Y film prepared in 10 min. (a) Film measured at −800 mV vs SCE, fits according to eq 4 (- - -) and eqs 4 and 5 (—); (b) film measured at 0 V vs SCE, fits according to eqs 2 and 4 with $\tau_n = 0.8$ s, $d = 0.8$ μm, $\alpha = 19\,700$ cm^{-1}, $R = 21$ Ω, and $C = 6.4$ μF.

However, if the same film (10 min deposition time) is measured at 0 V vs SCE, then it seems to behave like a nanoporous electrode as seen in the much lower f_{min} value and the absence of a surface recombination reaction typical for bulk electrodes. The low f_{min} value cannot be explained by a change in the *RC* constant, because a lower capacitance is expected at a more positive potential for an n-type electrode. Field-driven electron transport to the back-contact would be faster at more positive potentials. Therefore, slow electron transport by diffusion, which is typical for nanoporous electrodes, is found in this experiment. Consequently, the IMPS results are fitted rather well with a product of eqs 2 and 4 (Figure 4b). Average values of *R* and *C* derived from the fits in Figure 4a were used in these fits, while experimental values were inserted for *d*, τ_n, and α.[5] D_n and Φ_{inj} were adjustable parameters. It should be noted at this point that the experimental *d* value of 1.4 μm (Figure 1) was reduced by 0.6 μm to consider only the part of the film where no field-driven electron transport occurs, which will be discussed in more detail below. The fits gave D_n values of 4.8×10^{-6} cm^{-2} s^{-1} for the real component and 7.4×10^{-6} cm^{-2} s^{-1} for the imaginary component, which are in good accordance with a D_n value of 4×10^{-6} cm^{-2} s^{-1} which was reported previously for as-deposited ZnO/eosin Y films illuminated with the same light intensity through the back-contact.

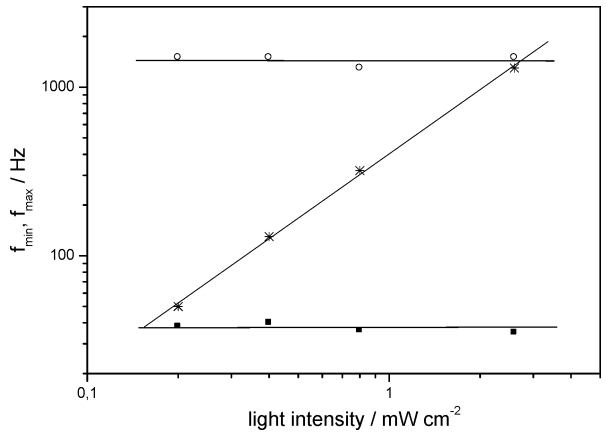

Figure 5. IMPS f_{min} and f_{max} values for a ZnO/eosin Y film prepared in 10 min: (○) f_{min} at −800 mV vs Ag/Ag$^+$; (■) f_{max} at −800 mV vs Ag/Ag$^+$; (∗) f_{min} at 0 mV vs Ag/Ag$^+$.

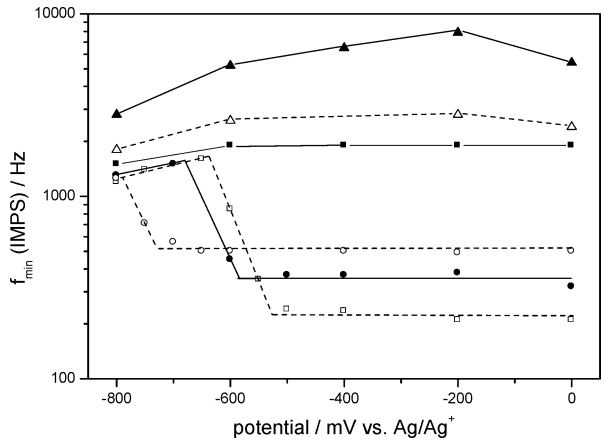

Figure 6. Potential dependence of the f_{min} values in the IMPS complex plane plots of readsorbed ZnO/eosin Y films of different film thicknesses. The films were electrodeposited in 2 (▲), 3 (△), 4 (■), 5 (□), 10 (●), and 20 min (○). The lines have no direct physical meaning and represent only a guide for the eye.

From the results of the IMPS fits, it can be concluded that f_{min} reflects either *RC* attenuation with $RC = 1/(2\pi f_{min})$ or electron diffusion with $\tau_D = 1/(2\pi f_{min})$, depending on the electrode potential. This is also seen in the light intensity dependence of f_{min} as shown for the film of 10 min deposition time in Figure 5. At −800 mV, a constant f_{min} is seen, which is expected if f_{min} reflects the *RC* constant, because both *R* and *C* should not depend on the light intensity in a first approximation. However, a clear increase of f_{min} with increasing light intensity is seen at 0 mV vs SCE. Such an increase is expected if f_{min} reflects τ_D, because electron traps will be filled up at higher light intensities, which leads to faster electron diffusion.

Figure 6 gives an overview of the potential dependence of f_{min} for films of different deposition times. From negative to positive potentials, the f_{min} values measured at films deposited in 3 and 4 min are similarly high and have a similar potential dependence as those of the film of 2 min deposition time. Therefore, it can be assumed that f_{min} reflects the *RC* constant in all measurements at these three films. The SEM micrograph of the film after a 2 min deposition time (Figure 2a) shows certain porosity, such that a higher surface area and capacitance is expected with increasing film thickness. This increasing *C* explains the decrease in f_{min}, provided that an electric field is present all over the films, such that the porous films behave like bulk electrodes.

However, from 4 to 5 min deposition times, a very drastic decrease in f_{min} occurs between −0.5 and 0 V vs SCE, which cannot be explained by a change in *C*. The much lower f_{min} value can rather be explained if it is assumed that it reflects slow electron transport by diffusion. It was seen in Figures 2b and 2c that the films become increasingly porous with increasing deposition time. This can be interpreted in a way that after 5 min deposition time the porosity of the film in its outer part has increased to an extent that an electric field is no longer present, which means that no space charge layer is formed at the interface between this part of the film and the electrolyte[16] and the electron diffusion in this part can be detected in the IMPS response. Interestingly, Figure 2b shows that the size of the ZnO domains in this part of the film (10−40 nm) is comparable to the size of crystallites usually used for dye-sensitized TiO_2 solar cells (e.g., Degussa P25).

If the film thickness is further increased (10 and 20 min deposition times), f_{min} becomes higher again (Figure 5). This can be explained by the higher average electron concentration in these films, which is caused by the higher overall surface area as also seen in the higher photocurrents (Figure 1). All films where f_{min} reflects electron diffusion toward positive potentials (i.e., films with deposition times of 5, 10, and 20 min) show a sharp increase of f_{min} toward negative potentials in the region between −0.5 and −0.8 V vs Ag/Ag$^+$. This would mean faster electron transport to the back-contact at more negative potentials, which appears odd at first sight. However, this result can be understood considering that in this potential region more and more electrons are injected into the nanoporous part of the film as the electrode potential approaches the position of the ZnO conduction band. The resulting increase in the electron concentration should lead to the filling of electron traps and therefore to faster diffusion of photogenerated electrons.

It can be expected that f_{min} increases until it reaches the value determined by the *RC* constant, while the electron transport presumably continues to become faster. This can be seen in the abrupt end of the increase for the films with 5 and 10 min deposition times at around −0.62 and − 0.64 V vs SCE (Figure 6). At −0.8 V vs SCE, all films with deposition times ≥5 min have the same f_{min}. Assuming that *R* is determined by the conducting back-contact, the capacitance that contributes to the *RC* constant is the same in all these films. It can be concluded that only the part of the film that is deposited in the first 4−5 min and where electron transport is field-driven contributes to this capacitance. Consequently, films with deposition times ≤4 min show a higher f_{min} value at −0.8 V due to their lower capacitance. Figure 7 shows this relationship between deposition time and capacitance, calculated from the f_{min} values and *RC* constants at −0.8 V vs SCE (Figure 6), assuming a resistance of 21 Ω as found in a previous section. It is estimated that the "bulky" part of the films is deposited in the first 4.5 min, which corresponds to a film thickness of about 0.6 μm (Figure 1). From a deposition time of 2 min until this point, an almost linear increase of the capacitance is found, indicating that the inner surface of the first 0.6 μm completely contributes to the capacitance.

The potential dependence of the f_{max} values is shown in Figure 8 for all films. The results are rather well-fitted by the exponential function

$$n_{surf} = n_{bulk} \exp\left(\frac{q(\Phi_{fb} - \Phi)}{kT}\right) \qquad (7)$$

where n_{surf} and n_{bulk} are the electron concentrations at the surface and in the bulk and $\Phi_{fb} - \Phi$ is the potential drop in the space

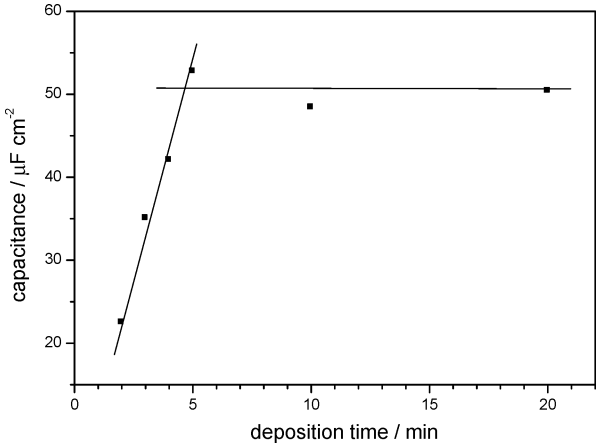

Figure 7. Capacitance of readsorbed ZnO/eosin Y films calculated from the results of the IMPS measurements at −0.8 mV vs SCE.

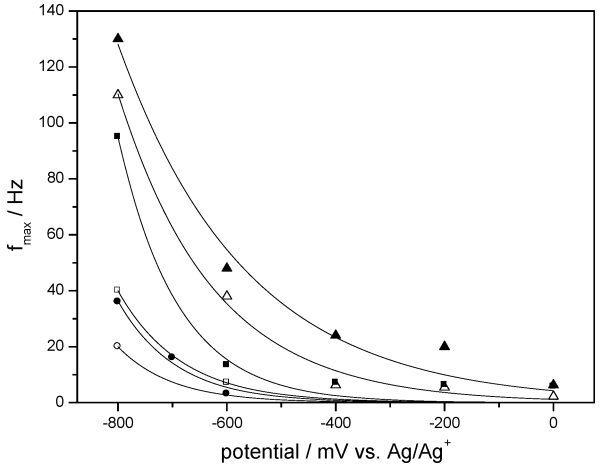

Figure 8. Potential dependence of f_{max} in the IMPS complex plane plots of readsorbed ZnO/eosin Y films of different film thicknesses. The films were electrodeposited in 2 (▲), 3 (△), 4 (■), 5 (□), 10 (●), and 20 min (○). The data were fitted with eq 7.

charge layer. n_{bulk} and ($\Phi_{fb} - \Phi$) were the variable parameters in this fit. k_{rec} is a pseudo-first-order rate constant that is proportional to n_{surf} (section 2). Although f_{max} reflects k_{rec} as well as k_{tr} (eq 6), k_{tr} can be assumed to be constant due to the constant electrolyte concentration, such that $k_{rec} \gg k_{tr}$ and f_{max} is proportional to k_{rec} and therefore to n_{surf} toward negative potentials in a first approximation.

Therefore, the experimental and fitting results in Figure 8 again prove that f_{max} describes the surface reactions of photogenerated holes at the surface of the "bulky" part of the film according to eq 6.

The question arises as to why, at a given potential, higher f_{max} values are obtained for thinner films. One explanation would be a negative shift of the flat-band potential with increasing film thickness, which would also provide an explanation as to why the increase of f_{min} starts at more negative potentials in Figure 6 for the film prepared in 20 min as compared to the films prepared in 10 and 5 min. However, such a shift in the flat-band potential would have to concern the inner, bulky part of the films, and the shift would have to happen after the actual deposition of this part, which is not expected. Furthermore, a shift in the flat-band potential could not be confirmed by measurements of Mott−Schottky plots (section 4.3). It is therefore more likely that the differences in f_{max} for films of different thicknesses are caused by differences in n_{bulk} according to eqs 7 and 8. Differences in n_{bulk} might be caused by the decreasing light intensity in the bulky part of the film with increasing film thickness.

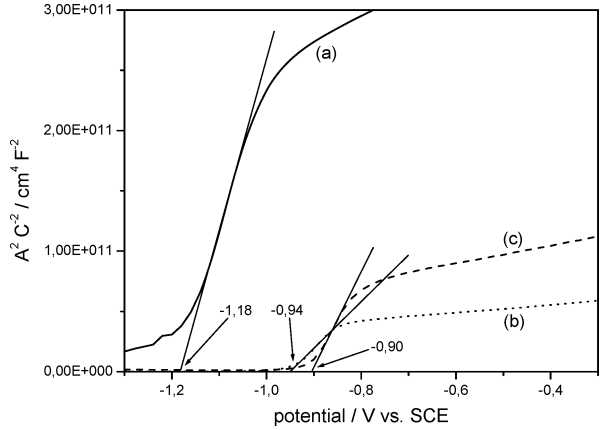

Figure 9. Typical Mott−Schottky plots of a ZnO/eosin Y film deposited in 20 min: (a) as-deposited; (b) after desorption of the dye; (c) after readsorption of eosin Y.

4.3. Comparison with Capacitance Measurements. Figure 9 shows a typical example for Mott−Schottky plots of an as-deposited film and the same film after desorption and readsorption of the dye. While the flat-band potentials around −0.9 V vs Ag/Ag$^+$ after desorption and readsorption of the dye are comparable with flat-band potentials reported for electrodeposited ZnO earlier,[17] much more negative flat-band potentials around −1.2 V vs Ag/Ag$^+$ are found for the as-deposited ZnO/eosin Y film. Since dye aggregates are present in this film, it is suggested that the latter value at least partly reflects the properties of the eosin Y. This becomes even more plausible if it is considered that the first reduction of eosin Y occurs at ca. −0.9 V vs SCE,[4] indicating a LUMO level of ca. −1.2 V on the Ag/Ag$^+$ scale. The much lower capacitance of the as-deposited film can also be explained by dye aggregation, as it leads to a (partial) blocking of the ZnO pores. In accordance with this interpretation, the highest capacitance is observed after desorption of the dye, while a slightly lower capacitance is again seen after the readsorption of the dye.

Separate capacitance measurements were made to verify the results of the IMPS measurements. Unfortunately, the measurements made with readsorbed films were not well reproducible and gave no clear trend if results for different film deposition times and measuring frequencies were compared. This is probably due to differences in the dye readsorption process, which seems to be not perfectly reproducible yet. Measurements at pure ZnO films after desorption of the dye showed a much better reproducibility. Some of the results are shown in Figure 10.

For comparison with the capacitances calculated from the IMPS response (Figure 7), values for −0.8 V vs SCE and 1 kHz in Figure 10 have to be considered, because the *RC* constants are in the range of 1 kHz and capacitances that are charged and discharged on a slower time scale will not contribute to the *RC* constant. Doing so, it is seen that the values shown in Figures 7 and 10 are in good agreement. For example, it is seen in Figure 7 as well as in Figure 10 for 1 kHz that the films deposited in 5 and 20 min have almost the same capacitance. However, this changes dramatically when the frequency is lowered. While the capacitance of the film with a 5 min deposition time increases only slightly, the film with a 20 min deposition time reaches a 5 times higher capacitance at 1 Hz. This matches quite well the increase in the film thickness by a factor of 4. In accordance with the discussion of the IMPS

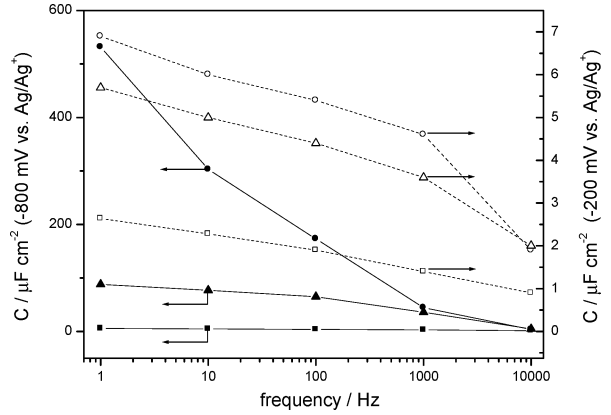

Figure 10. Results of capacitance measurements at −0.2 V mV vs Ag/Ag^+ (open symbols, dashed lines, right scale) and −0.8 V vs SCE (solid symbols, solid lines, left scale). The lines are shown for clarity only. The measurements were made at films prepared in 2 (□,■), 5 (△,▲), and 20 min (○,●).

results (section 4.2), it is again concluded that in the thick film (20 min deposition time) only the space charge capacitance in the bulky part of the film is seen at 1 kHz, while the whole film including the field-free part is charged and discharged at 1 Hz. The slow charging and discharging of the field-free part by electron diffusion explains why the *RC* constants are the same for all films with deposition times ≥5 min, while the overall capacitance, which includes the space charge capacitance C_{sc} as well as the "chemical capacitance" C_{ch} of the nanoporous part, further increases with the film thickness.

Capacitances shown for −0.2 V vs Ag/Ag^+ in Figure 10 are considerably lower than those measured at −0.8 V vs Ag/Ag^+, which is in accordance with the higher f_{min} value for the thin films in Figure 6. Interestingly, all films show only a slight increase in the capacitance if the frequency is lowered from 1 kHz to 1 Hz. This means that at −0.2 V vs Ag/Ag^+ the field-free parts of the films are not charged and discharged or only to a small extent.

5. Conclusions

The electrochemically self-assembled ZnO/dye hybrid films investigated in this study show a porosity that increases with deposition time and film thickness, yielding films that consist of two parts with different properties. The first part, deposited in 4−5 min (ca. 0.6 μm) has a rather low porosity, leading to bulk electrode properties such as field-driven electron transport and surface recombination of photogenerated minority carriers with majority carriers. Thicker films have an outer part with a higher porosity that is field-free and where electron transport takes place by diffusion.

While the present study confirms our earlier results concerning applications of ZnO/eosin Y films in dye-sensitized solar cells, they are also of much interest in view of their use in supercapacitors. A comparison of the values of up to ca. 540 μF cm^{-2} (Figure 10) with typical values of 150−250 μF cm^{-2} for metal oxide films used for supercapacitors[18] are in favor of the material investigated in this study. The film prepared in 5 min has a much lower capacitance at 1 Hz compared to thicker films but still a comparatively high capacitance of ca. 36 μF cm^{-2} at 1 kHz. This is quite high compared to 15 μF cm^{-2}, which is a typical value for the carbon electrodes that are often used in supercapacitors.[18] The less porous (bulky) part of the ZnO/eosin Y electrodes therefore seems to be a material that shows both a fast, field-driven electron transport and a rather high surface area and capacitance, making this material suitable for fast supercapacitors.

Acknowledgment. This study, including a 1 month stay of T.O. at Gifu University, was in part financed by the Industrial Technology Research Grant Program 2004 from the New Energy and Industrial Technology Development Organization (NEDO) of Japan (01B64002c). We thank H. Tada and the Ministry of Education, Culture, Sports, Science and Technology of Japan for access to SEM equipment at the Institute for Molecular Science (IMS), Okazaki, Japan.

References and Notes

(1) Yoshida, T.; Minoura, H. *Adv. Mater.* **2000**, *12*, 1219.
(2) Yoshida, T.; Terada, K.; Schlettwein, D.; Oekermann, T.; Sugiura T.; Minoura, H. *Adv. Mater.* **2000**, *12*, 1214.
(3) Yoshida, T.; Oekermann, T.; Okabe, K.; Schlettwein, D.; Funabiki, K.; Minoura, H. *Electrochemistry* **2002**, *70*, 470.
(4) Yoshida, T.; Pauporté, T.; Lincot, D.; Oekermann, T.; Minoura, H. *J. Electrochem. Soc.* **2003**, *150*, C608.
(5) Oekermann, T.; Yoshida, T.; Minoura, H.; Wijayantha, K. G. U.; Peter, L. M. *J. Phys. Chem. B* **2004**, *108*, 8364.
(6) Yoshida, T.; Iwaya, M.; Ando, H.; Oekermann, T.; Nonomura, K.; Schlettwein, D.; Wöhrle, D.; Minoura, H. *Chem. Commun.* **2004**, *400*.
(7) Gu, Z. H.; Fahidy, T. Z. *J. Electrochem. Soc.* **1999**, *146*, 156.
(8) Fabregat-Santiago, F.; Garcia-Belmonte, G.; Bisquert, J.; Bogdanoff, P.; Zaban, A. *J. Electrochem. Soc.* **2003**, *150*, E293.
(9) Conway, B. E. *Electrochemical Supercapacitors: Scientific Fundamentals and Technological Applications*; Kluwer Academic/Plenum Publishing: New York, 1999.
(10) Södergren, S.; Hagfeldt, A.; Olsson, J.; Lindquist, S. E. *J. Phys. Chem.* **1994**, *95*, 5522.
(11) Wang, P.; Zakeeruddin, S. M.; Moser, J. E.; Nazeeruddin, M. K.; Sekiguchi, T.; Grätzel, M. *Nat. Mater.* **2003**, *2*, 402.
(12) Peter, L. M.; Vanmaekelbergh, D. *Advances in Electrochemical Science and Engineering*; Alkire, R. C., Kolb, D. M., Eds.; Wiley-VCH: Weinheim, Germany, 1999; Vol. 6.
(13) Vanmaekelbergh, D.; de Jongh, P. *J. Phys. Chem. B* **1999**, *103*, 747.
(14) Dloczik, L.; Ileperuma, O.; Lauermann, I.; Peter, L. M.; Ponomarev, E. A.; Redmond, G.; Shaw, N. J.; Uhlendorf, I. *J. Phys. Chem. B* **1997**, *101*, 10281.
(15) Franco, G.; Peter, L. M.; Ponomarev, E. A. *Electrochem. Commun.* **1999**, *1*, 61.
(16) Cahen, D.; Grätzel, M.; Guillemoles, J. F.; Hodes, G. *Electrochemistry of Nanomaterials*; Hodes, G., Ed.; Wiley-VCH: Weinheim, Germany, 2001.
(17) Oekermann, T.; Yoshida, T.; Schlettwein, D.; Sugiura, T.; Minoura, H. *Phys. Chem. Chem. Phys.* **2001**, *3*, 3387.
(18) Shukla, A. K.; Sampath, S.; Vijayamohanan, K. *Curr. Sci.* **2000**, *79*, 1656.